Direct Observation of Rapid Discrete Spectral Dynamics in Single Colloidal CdSe-CdS Core-Shell Quantum Dots

Direct Observation of Rapid Discrete Spectral Dynamics in Single Colloidal CdSe-CdS Core-Shell Quantum Dots

Andrew P. Beyler, Lisa F. Marshall, Jian Cui, Xavier Brokmann, and Moungi G. Bawendi*

Department of Chemistry, Massachusetts Institute of Technology, Cambridge, Massachusetts 02139, USA

(Received 25 January 2013; published 25 October 2013)

We measure the anomalous spectral diffusion of single colloidal quantum dots over eight temporal decades simultaneously by combining single-molecule spectroscopy and photon-correlation Fourier spectroscopy. Our technique distinguishes between discrete and continuous dynamics and directly reveals that the quasicontinuous spectral diffusion observed using conventional spectroscopy is composed of rapid, discrete spectral jumps. Despite their multiple time scales, these dynamics can be captured by a single mechanism whose parameters vary widely between dots and over time in individual dots.

DOI: 10.1103/PhysRevLett.111.177401 PACS numbers: 78.67.Bf, 42.50.Ar, 82.37.Vb

Disordered systems such as glasses, supercooled liquids, and proteins exhibit intricate collective dynamics on time scales spanning many orders of magnitude. Multi-time-scale techniques like dielectric spectroscopy and spectral hole burning have therefore proven invaluable for elucidating the properties of these phenomena [1]. However, ensemble techniques are not easily applied to the investigation of synthetic nanostructures because structural polydispersity can lead to highly heterogeneous dynamical properties. As a result, many processes in nanoscale systems remain poorly understood despite their relevance for practical applications.

The local electric field dynamics in colloidal quantum dots (CQDs) and other semiconductor nanostructures are a particularly notable multi-time-scale phenomenon because they are interrelated with CQD fluorescence intermittancy [2] and cause spectral diffusion via the quantum-confined Stark effect [3]. Prevailing theories have attributed these field fluctuations to either the trapping and migration of carriers in a manifold of heterogeneous trap states at the shell-ligand interface [4–7] or to the rearrangement of the CQD ligands [8], but the dearth of suitable multi-time-scale probes for CQD spectral diffusion has left its physical cause an open question.

Spectral dynamics in CQDs have generally been studied using single-molecule spectroscopy because it can unambiguously reveal individual spectral trajectories free of ensemble averaging. Using this technique, CQD spectral diffusion has been found to obey a continuous subdiffusion power law on the time scale of seconds with a highly variable exponent [9]. Two investigations have also reported indirect evidence that this behavior may actually be quasicontinuous, composed of discrete photoinduced jumps on faster time scales [4,10]. Nevertheless, these fast, discrete spectral jumps are not usually observable using single-molecule spectroscopy because of its inherent tradeoff between temporal resolution, spectral resolution, and signal-to-noise ratio. Previous studies using spectral hole burning [11,12] and photon-correlation Fourier spectroscopy (PCFS) [13,14] have not leveraged their higher temporal resolution to observe this discrete behavior. Moreover, neither of these experiments can measure dynamics on time scales longer than hundreds of milliseconds. No single existing technique can measure the full range of spectral dynamics in CQDs.

In this Letter, we use PCFS to directly observe rapid, discrete spectral diffusion events in CQDs. This effort demonstrates the utility of PCFS in revealing the mechanistic details of subsecond processes in heterogeneous systems. Then, we combine PCFS with conventional single-molecule spectroscopy to form a single-molecule experiment that can simultaneously measure spectral dynamics across 8 orders of magnitude in time ranging from microseconds to hundreds of seconds. We use this technique to observe CQD spectral diffusion across its discrete and quasicontinuous regimes, forming a unified description of this phenomenon.

Photon-correlation Fourier spectroscopy, described theoretically and experimentally elsewhere [13–15], measures the evolution of a single-molecule spectrum by monitoring the intensity anticorrelation produced by spectral coherence at the outputs of an interferometer. This approach fundamentally changes the way spectral information is compiled compared to conventional spectroscopy. In the single-photon counting paradigm, rather than histogramming the energy of photons during an integration time to form a spectrum, PCFS histograms the energy difference ζ between pairs of photons with some time separation τ. In essence, by replacing the intensity measurement of Fourier transform spectroscopy with Hanbury Brown-Twiss-style photon correlation, PCFS disentangles the temporal resolution of a measurement from its integration time. High signal-to-noise, temporal resolution, and spectral resolution can all be achieved simultaneously by increasing the duration of the experiment.

The spectral quantity produced by this histogramming procedure is the spectral correlation,

$$p(\zeta,\tau) = \left\langle \int_{-\infty}^{\infty} s(\omega,t)s(\omega+\zeta,t+\tau)d\omega \right\rangle_t, \quad (1)$$

where $s(\omega, t)$ is the single-molecule spectrum at time t and $\langle\cdots\rangle_t$ denotes a time average. Whereas an integrated spectrum contains a single spectral diffusion trajectory, $p(\zeta, \tau)$ surveys the progress of all possible trajectories over the time τ between photon arrivals. As $\tau \to 0$, $p(\zeta, \tau)$ reduces to the autocorrelation of the homogeneous spectrum, since both photons are drawn from the same static distribution. Then, as τ increases, $p(\zeta, \tau)$ broadens as it is convolved with the broadening probability density function of spectral diffusion.

Previous investigations using PCFS did not scrutinize how the shape of $p(\zeta, \tau)$ evolves in time [13,14]. We show here that the evolving shape of $p(\zeta, \tau)$ is sensitive to the mechanistic details of spectral dynamics on time scales inaccessible to other single-molecule methods. Whereas distinguishing between discrete and continuous diffusion mechanisms is impossible using single-point correlation experiments [16–18] and requires complicated statistical inference using spectrum-based experiments [10], these types of spectral diffusion each have their own distinct qualitative footprint in $p(\zeta, \tau)$.

Figure 1(a) shows the temporal evolution of $p(\zeta, \tau)$ for a spectrum diffusing according to a continuous Wiener process (i.e., Brownian motion). The probability density function is a single Gaussian whose FWHM broadens as $\tau^{0.5}$ [Fig. 1(c), blue] [19]. In contrast, Fig. 1(b) shows the $p(\zeta, \tau)$ for a spectrum diffusing according to a discrete Gaussian random walk process governed by Poisson statistics. The discrete nature of the Poisson model manifests itself in $p(\zeta, \tau)$ as a population transfer between two subpopulations of photon pairs. At short τ, $p(\zeta, \tau)$ is dominated by the population of photon pairs without a diffusion event between them, which contribute a narrow "nondiffused" distribution. Then, as τ increases, probability density is transferred to the population of photon pairs with one or more diffusion event between them. These photon pairs contribute a broad non-Gaussian "diffused" distribution, which broadens and eventually becomes Gaussian as multiple diffusion events become common [Fig. 1(c), black]. In practice, the population transfer from the nondiffused to the diffused distribution may not be as obvious as in Fig. 1(b). Nevertheless, in cases where the two distributions are not clearly resolved, this population transfer may still produce a characteristic inflection point in the width of $p(\zeta, \tau)$ [Fig. 1(c), see arrow], which is evidence for discrete diffusion.

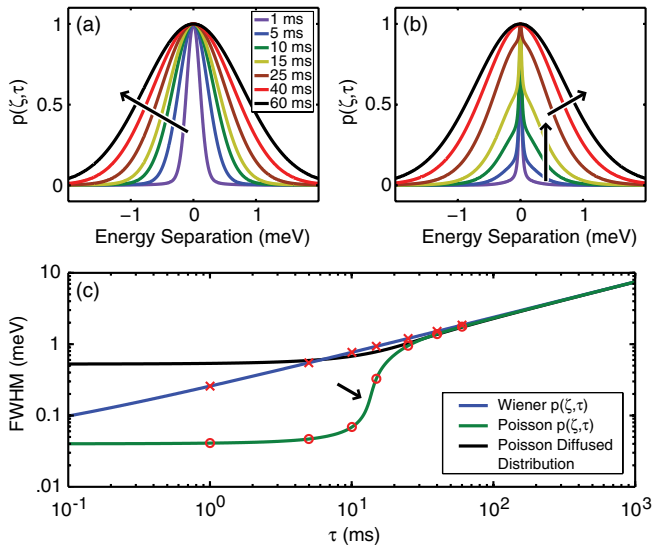

FIG. 1 (color online). Simulated $p(\zeta, \tau)$ for a fluorophore undergoing (a) continuous Wiener spectral diffusion (Brownian motion) and (b) discrete Gaussian random walk governed by Poisson jump statistics. Model parameters are given in the Supplemental Material [20]. (c) FWHM of the $p(\zeta, \tau)$ corresponding to these continuous (blue) and discrete (green) processes. The τ's from (a) and (b) are marked with ×'s and ○'s, respectively. The FWHM of the diffused contribution to the Poisson $p(\zeta, \tau)$ is plotted in black. The arrow highlights the inflection point characteristic of discrete mechanisms.

The central limit theorem causes these two spectral diffusion models to produce identical, indistinguishable results in the long τ limit accessible using conventional techniques. However, if rapid spectral diffusion occurs via discrete photoinduced events as proposed, it will be reflected in the PCFS spectral correlation.

Our implementation of PCFS integrates several experimental advances from our related work on solution phase PCFS [21,22]. Here, we use an upright epifluorescence microscope with a cryostat operating at 4 K and we divert 10% of our signal to a spectrometer to monitor the integrated spectrum during the experiment. We use an empirical correction to account for detector afterpulsing [23], which would otherwise cause $p(\zeta, \tau)$ to artificially narrow on submillisecond time scales. Our samples, CdSe/(8 ML [24])CdS core [25]-shell [26] particles, exhibit room temperature emission centered at 640 nm and were chosen for their bright and stable fluorescence. Finally, the parameters of the PCFS experiment are optimized to focus exclusively on zero-phonon line emission.

The $p(\zeta, \tau)$ of a single CQD is presented in Fig. 2(a) and baseline subtracted and rescaled to emphasize changes in shape in Fig. 2(b). Two different temporal regimes are evident (see arrows). In the discrete regime, a narrow distribution corresponding to a 20 μeV homogeneous linewidth yields to a broad non-Gaussian 200 μeV distribution. Then, when the nondiffused distribution vanishes as $p(\zeta, \tau)$ reaches the quasicontinuous regime around $\tau =$ 5 ms, the diffused distribution continues to broaden and begins to adopt a more Gaussian line shape. The correspondence between Fig. 2(b) and the Poisson model in Fig. 1(b) confirms that rapid spectral diffusion in CQDs occurs through a discrete mechanism.

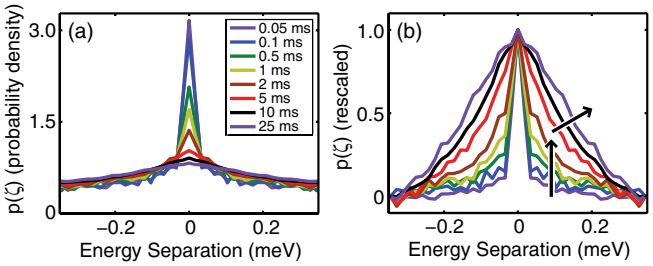

FIG. 2 (color online). $p(\zeta, \tau)$ of a single CQD (a) normalized by area and (b) baseline subtracted and rescaled. Arrows highlight the transition from discrete to quasicontinuous diffusion. The FWHM of $p(\zeta, \tau)$ is provided in the Supplemental Material [20].

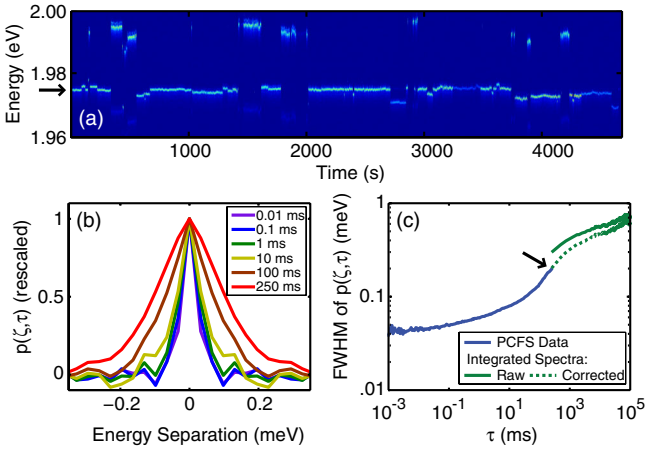

FIG. 3 (color online). Simultaneously measured (a) time series of integrated spectra. (b) $p(\zeta, \tau)$ corresponding to the emission from 1.975 eV. (c) FWHM of $p(\zeta, \tau)$ calculated from PCFS (blue) and time series (green) data. The dotted green line is corrected for the 91 μeV peak-fitting instrument function and the arrow highlights the inflection point produced by discrete diffusion.

However, PCFS alone cannot be used to measure spectral dynamics throughout both the discrete and quasicontinuous regimes because its survey of diffusion trajectories loses statistical significance after hundreds of milliseconds. To extend our measurement into the quasicontinuous regime, we can incorporate the CCD-based spectral data collected during the PCFS experiment using an analysis similar to that of Plakhotnik and Walser [27]. As shown in the Supplemental Material [20], $p(\zeta, \tau)$ can be approximated from the integrated data by

$$p(\zeta, \tau) \propto a(\zeta', T) * h(\zeta', \tau), \tag{2}$$

where $a(\zeta', T)$ is the autocorrelation of an average spectral frame integrated for time T (in this case, 250 ms), $h(\zeta', \tau)$ is the histogram of the energy shifts between pairs of frames separated by τ, and $*$ denotes a convolution in ζ'. Equation (2) reflects our intuitive description of $p(\zeta, \tau)$, where $a(\zeta', T)$ is analogous to the autocorrelation of the homogeneous line shape and $h(\zeta', \tau)$ is analogous to the probability density function of the spectral diffusion.

This compound experiment is applied to a different single CQD in Fig. 3. In addition to the sub-meV spectral dynamics observed with PCFS, the conventional spectrum also exhibits large spectral jumps over tens of meV and smaller spectral jumps over single meV [Fig. 3(a)]. Early investigations of single CQD cores reported discrete spectral jumps over tens of meV caused by carrier trapping in the environment of the CQD [6,28]. We attribute the smaller spectral shifts to this phenomenon as the magnitude of this effect should be reduced by the CdS shell. Meanwhile, the stratification of the large spectral jumps into two distinct spectral positions separated by $\sim$20 meV is consistent with recent reports of positive trion formation [29,30]. Because core charging affects the fluorescence intensity and integrated linewidth of the CQD (Fig. S3 of Supplemental Material [20]), we exclusively measure the emission at 1.975 eV [Fig. 3(a), see arrow]. The resulting $p(\zeta, \tau)$ is shown in Fig. 3(b) and its FWHM across both data sets is plotted in Fig. 3(c). The 91 μeV offset between the FWHM of the PCFS and integrated spectra $p(\zeta, \tau)$ is attributed to uncertainty in the center frequency of the spectrum caused by shot noise and CCD read noise and is removed to produce the dotted trace.

The results in Fig. 3 are consistent with those from Fig. 2. Although the population transfer between the diffused and nondiffused distributions is less clearly illustrated, the sharpness of $p(\zeta, \tau)$ implies the persistence of a nondiffused distribution and the FWHM of $p(\zeta, \tau)$ reaches an inflection point as that sharpness vanishes [Fig. 3(c), see arrow]. Then, beyond 1 s, the FWHM of $p(\zeta, \tau)$ broadens linearly on the log-log plot in Fig. 3(c) with a slope of 0.13, consistent with the power law subdiffusion behavior reported previously [9]. This slow transition to quasicontinuous spectral diffusion suggests wide variability in diffusion properties between CQDs. Whereas this CQD reaches the quasicontinuous regime at 1 s, the CQD from Fig. 2 reaches the quasicontinuous regime at 25 ms.

By tracking the evolution of $p(\zeta, \tau)$ across both the discrete and quasicontinuous regimes simultaneously, we reveal the transition between these disparate dynamical regimes. The correspondence between Fig. 3(c) and the Poisson model in Fig. 1(c) illustrates that the observed behavior over eight temporal decades can be captured by a single discrete mechanism. However, there are two key deviations between this spectral behavior and the Poisson model. First, the persistence of a nondiffused distribution in $p(\zeta, \tau)$ over several decades in time and the minimal curvature in inflection point feature in Fig. 3(c) suggest long-tail discrete jump kinetics rather than Poissonian first-order kinetics. Multi-time-scale kinetics have been explained in CQD blinking by temporal variations in the trapping rate of carriers from the core of the CQD [31]; such temporal variations may be at play here. Second, the

power law exponent in the quasicontinuous regime is less than 0.5. This subdiffusion implies either a correlation between jump events [8] or a confining potential, neither of which exist in the Poisson model.

Finally, we turn to the effect of carrier trapping in the vicinity of the CQD on spectral diffusion. Carrier trapping induces the smaller spectral shifts from Fig. 3(a) via the quantum-confined Stark effect. Given the second-order nature of this interaction, the net changes in local electric field produced by carrier trapping are known to inherently change the magnitude of spectral diffusion [3]. However, we demonstrate here that carrier trapping also induces fundamental changes in the discrete jump dynamics of spectral diffusion.

The $p(\zeta, \tau)$ corresponding to two spectral positions of another CQD [Fig. 4(a)], I and II, are presented in Fig. 4(b) and 4(c), respectively. Both $p(\zeta, \tau)$ reflect the discrete diffusion of a $\sim$15 μeV homogeneous spectrum, as shown from the evolving shape of the $p(\zeta, \tau)$ of II and from the inflection point in the FWHM of the $p(\zeta, \tau)$ of I [Fig. 4(d), see arrow]. Again, the persistence of the nondiffused distribution over several decades in II supports long-tail discrete kinetics. Then, at long τ, both I and II obey quasicontinuous power law subdiffusion. The clear distinction between the diffused and nondiffused distributions in

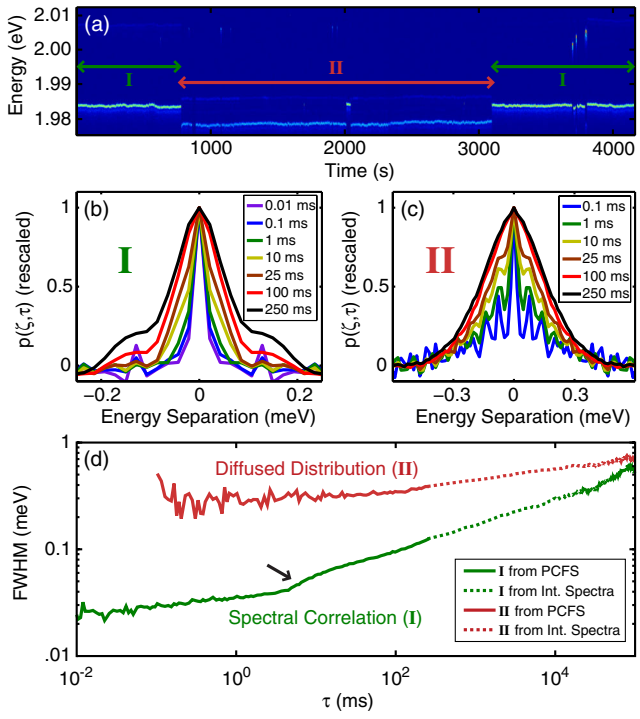

FIG. 4 (color online). (a) Time series of integrated spectra revealing two spectral positions I and II. (b)/(c) $p(\zeta, \tau)$ for I and II, respectively. (d) FWHM of the $p(\zeta, \tau)$ of I (green) and FWHM of the diffused distribution of II (red). Solid lines indicate PCFS, dotted lines indicate time series data with instrument function correction, and the arrow highlights the inflection point produced by discrete diffusion.

II also allows us to compare the evolution of the width of the diffused distribution [Fig. 4(d)] to the Poisson model [Fig. 1(c), black]. Both reach a plateau at short τ, produced in the Poisson model by independence between the magnitudes of jump events and the time between jump events.

The $p(\zeta, \tau)$ for I and II differ in several quantitative details. Even in the 0.1 ms cross section of II's $p(\zeta, \tau)$, the integrated area of the diffused contribution is already much greater than that of the nondiffused contribution [Fig. 4(c)]. This indicates that discrete diffusion events at II occur more frequently than they do at I. Their quasicontinuous power law broadening at long τ also feature different exponents, 0.11 versus 0.24, and prefactors, 33 versus 200 μeV. These parameters report on the degree of correlation between jump events and the effective diffusion constant of spectral diffusion, respectively. The significant changes in the rapid spectral dynamics across charge-trapping events represent a previously unreported interplay between these phenomena.

Both trapped carrier and ligand rearrangement theories are consistent with our observations of discrete spectral diffusion, long-tail kinetics, and quasicontinuous subdiffusion. On one hand, the trapped carrier theory elegantly rationalizes the interplay between spectral diffusion and carrier trapping shown in Fig. 4 because carrier trapping changes the number of peripheral charges responsible for spectral diffusion. This theory also better explains order-of-magnitude variations in the rate of spectral diffusion events between CQDs because spectral dynamics are defined by the location of a few trapped carriers in a heterogeneous manifold, rather than by the ensemble dynamics of the ligand shell. On the other hand, little is known about the manifold of surface trap states in CQDs and whether carriers can diffuse through it. The ligand rearrangement theory proposes a straightforward physical mechanism for spectral diffusion, which can rationalize the power law subdiffusion seen in Figs. 3 and 4 based on the structural similarity between the disordered ligand shell and polymers. Nevertheless, we note that the perturbation of ligand dipoles 5.4 nm from the center of the CQD is unlikely to produce the discrete spectral shifts of 50–200 μeV we observe via the width of the diffused distribution of the spectral correlation. These considerations lead us to suggest a hybrid theory, where spectral diffusion is caused by the perturbation of trapped carriers by ligand rearrangement.

In conclusion, we have directly observed that the fast spectral dynamics of CQDs occurs through rapid discrete spectral jumps, which average to give rise to quasicontinuous subdiffusion on longer time scales. These spectral dynamics can be captured by a single discrete mechanism whose jump kinetics, effective diffusion constant, and quasicontinuous broadening exponent vary both between CQDs and over time in an individual CQD. Our data, measured over 8 orders of magnitude in time, crystallize

the features that must be captured in physical models for spectral diffusion in CQDs. Furthermore, our results demonstrate the unique utility of the single-molecule spectral correlation as a model-independent probe of spectral dynamics in heterogeneous systems.

This research was supported by the U.S. Department of Energy, Office of Basic Energy Sciences, Division of Materials Sciences and Engineering under Grant No. DE-FG02-07ER46454. We thank O. Chen for samples. J. C. gratefully acknowledges support from the NSF-GRFP.

*mgb@mit.edu

[1] H. Frauenfelder, *The Physics of Proteins: An Introduction to Biological Physics and Molecular Biophysics*, edited by S. S. Chan and W. S. Chan (Springer, New York, 2010).
[2] R. G. Neuhauser, K. T. Shimizu, W. K. Woo, S. A. Empedocles, and M. G. Bawendi, Phys. Rev. Lett. **85**, 3301 (2000).
[3] S. A. Empedocles and M. G. Bawendi, Science **278**, 2114 (1997).
[4] S. A. Empedocles and M. G. Bawendi, J. Phys. Chem. B **103**, 1826 (1999).
[5] J. Müller, J. M. Lupton, A. L. Rogach, J. Feldmann, D. V. Talapin, and H. Weller, Phys. Rev. Lett. **93**, 167402 (2004).
[6] J. Müller, J. M. Lupton, A. L. Rogach, J. Feldmann, D. V. Talapin, and H. Weller, Phys. Rev. B **72**, 205339 (2005).
[7] D. E. Gómez, J. van Embden, and P. Mulvaney, Appl. Phys. Lett. **88**, 154106 (2006).
[8] M. J. Fernée, T. Plakhotnik, Y. Louyer, B. N. Littleton, C. Potzner, P. Tamarat, P. Mulvaney, and B. Lounis, J. Phys. Chem. Lett. **3**, 1716 (2012).
[9] T. Plakhotnik, M. J. Fernée, B. Littleton, H. Rubinsztein-Dunlop, C. Potzner, and P. Mulvaney, Phys. Rev. Lett. **105**, 167402 (2010).
[10] M. J. Fernée, B. Littleton, T. Plakhotnik, H. Rubinsztein-Dunlop, D. E. Gómez, and P. Mulvaney, Phys. Rev. B **81**, 155307 (2010).
[11] P. Palinginis and H. Wang, Appl. Phys. Lett. **78**, 1541 (2001).
[12] P. Palinginis, S. Tavenner, M. Lonergan, and H. Wang, Phys. Rev. B **67**, 201307 (2003).
[13] L. Coolen, X. Brokmann, P. Spinicelli, and J.-P. Hermier, Phys. Rev. Lett. **100**, 027403 (2008).
[14] L. Coolen, P. Spinicelli, and J.-P. Hermier, J. Opt. Soc. Am. B **26**, 1463 (2009).
[15] X. Brokmann, M. G. Bawendi, L. Coolen, and J.-P. Hermier, Opt. Express **14**, 6333 (2006).
[16] G. Sallen, A. Tribu, T. Aichele, R. André, L. Besombes, C. Bougerol, M. Richard, S. Tatarenko, K. Kheng, and J.-P. Poizat, Nat. Photonics **4**, 696 (2010).
[17] M. Abbarchi, T. Kuroda, T. Mano, M. Gurioli, and K. Sakoda, Phys. Rev. B **86**, 115330 (2012).
[18] J. Wolters, N. Sadzak, A. W. Schell, T. Schröder, and O. Benson, Phys. Rev. Lett. **110**, 027401 (2013).
[19] In practice, this expression will be convolved with the autocorrelation of the homogeneous line shape. See Supplemental Material [20] for more information.
[20] See Supplemental Material at http://link.aps.org/supplemental/10.1103/PhysRevLett.111.177401 for theoretical and experimental details.
[21] L. F. Marshall, J. Cui, X. Brokmann, and M. G. Bawendi, Phys. Rev. Lett. **105**, 053005 (2010).
[22] J. Cui, A. P. Beyler, L. F. Marshall, O. Chen, D. K. Harris, D. D. Wanger, X. Brokmann, and M. G. Bawendi, Nat. Chem. **5**, 602 (2013).
[23] M. Zhao, L. Jin, B. Chen, Y. Ding, H. Ma, and D. Chen, Appl. Opt. **42**, 4031 (2003).
[24] Here, a single monolayer (ML) is defined as the c lattice constant in the CdS unit cell (0.676 nm).
[25] O. Chen, X. Chen, Y. Yang, J. Lynch, H. Wu, J. Zhuang, and Y. Cao, Angew. Chem., Int. Ed. **47**, 8638 (2008).
[26] O. Chen, J. Zhao, V. P. Chauhan, J. Cui, C. Wong, D. K. Harris, H. Wei, H.-S. Han, D. Fukumura, R. K. Jain, and M. G. Bawendi, Nat. Mater. **12**, 445 (2013).
[27] T. Plakhotnik and D. Walser, Phys. Rev. Lett. **80**, 4064 (1998).
[28] S. A. Empedocles, D. J. Norris, and M. G. Bawendi, Phys. Rev. Lett. **77**, 3873 (1996).
[29] M. J. Fernée, C. Sinito, Y. Louyer, C. Potzner, T.-L. Nguyen, P. Mulvaney, P. Tamarat, and B. Lounis, Nat. Commun. **3**, 1287 (2012).
[30] Y. Louyer, L. Biadala, P. Tamarat, and B. Lounis, Appl. Phys. Lett. **96**, 203111 (2010).
[31] P. Frantsuzov, M. Kuno, B. Jankó, and R. A. Marcus, Nat. Phys. **4**, 519 (2008).